Journal of Applied Physics

RESEARCH ARTICLE | APRIL 08 2025

A novel hybrid 2D-FDTD-PML and Nelder–Mead methods for estimating liquid complex permittivity using a rectangular waveguide

Omaima Talmoudi ; Lahcen Ait Benali; Jaouad Terhzaz; Abdelwahed Tribak; Tomás Fernández-Ibáñez

J. Appl. Phys. 137, 144501 (2025)
https://doi.org/10.1063/5.0264173

Journal of Applied Physics ARTICLE pubs.aip.org/aip/jap

A novel hybrid 2D-FDTD-PML and Nelder–Mead methods for estimating liquid complex permittivity using a rectangular waveguide

Cite as: J. Appl. Phys. **137**, 144501 (2025); doi: 10.1063/5.0264173
Submitted: 9 February 2025 · Accepted: 20 March 2025 ·
Published Online: 8 April 2025

Omaima Talmoudi,[1,a)] Lahcen Ait Benali,[2] Jaouad Terhzaz,[2] Abdelwahed Tribak,[1] and Tomás Fernández-Ibáñez[3]

AFFILIATIONS

[1]Institut national des postes et télécommunications, Rabat, Morocco
[2]Centre Régional des Métiers de l'Education et de la Formation, Casablanca, Morocco
[3]Departamento de Ingeniería de Comunicaciones, Universidad de Cantabria, Santander, Spain

[a)]**Author to whom correspondence should be addressed:** omaimatalmoudi@gmail.com

ABSTRACT

This paper introduces a novel approach for estimating the complex permittivity of liquids using a rectangular waveguide. The approach uses the finite difference time domain (FDTD) method, enhanced by perfectly matched layer (PML) boundary conditions to minimize reflections and ensure accurate calculation of the S-parameters. To address the challenge of sealing the waveguide ends, the waveguide is sealed at both ends with a resin sample of known complex permittivity, incorporating a small hole in the waveguide for liquid insertion. A Nelder–Mead optimization algorithm is then used in conjunction with the FDTD-PML method to estimate the complex permittivity of the liquid by iteratively comparing the calculated and measured S-parameters. Validated in the X-band frequency range, this technique demonstrates accurate estimation of the complex permittivity of liquid dielectric materials and offers a reliable means for liquid characterization.

I. INTRODUCTION

The study of liquid materials, particularly in the microwave frequency range, remains a key area of research due to its wide range of applications in telecommunications, environmental monitoring, and biomedical research. Within this context, the X-band is especially significant because of its versatility in these fields.[1,2] The dielectric properties of liquids, such as permittivity and loss tangent, provide essential insights into how these materials interact with electric fields and dissipate energy.[3] A deep understanding of these interactions is crucial for optimizing systems that utilize liquid-based materials.

Waveguide measurement techniques, especially those using rectangular waveguides, have been explored for material characterization. However, their practical application to liquids is often hampered by sealing difficulties.[4,5] To address the sealing issue and fill the rectangular waveguide with a liquid sample, both ends of the waveguide are sealed using two plugs with identical dielectric properties and lengths.[6,7] This configuration significantly complicates the complete modal analysis required for accurately determining the dielectric properties of the liquid material enclosed between the plugs. In this situation, using a numerical method, such as the finite-difference time-domain (FDTD) technique,[8] proves simpler than modal analysis for characterizing liquid dielectric materials. Moreover, the proposed numerical approach can be easily generalized to cases where the plugs have different permittivities or thicknesses.[9–11]

Recent studies have increasingly focused on improving characterization techniques in the microwave frequency range. Computational advancements have significantly enhanced the precision of dielectric property extraction from experimental data. The integration of machine learning algorithms, genetic algorithms, and electromagnetic simulations has resulted in more accurate and reliable results, enabling a deeper analysis of complex liquid systems.[12–14]

In this research, we focus on a comprehensive analysis of the dielectric properties of common liquids in the X-band frequency range, addressing challenges related to sealing and confinement within waveguides. To overcome these difficulties, we designed a rectangular waveguide setup with resin fixed at the boundaries to provide a controlled and leak-proof environment for liquid characterization, and a hole in the top surface. The rectangular waveguide was chosen because of its ability to characterize materials over a wide range of frequencies and to provide simple and effective measurements. Its simplicity and ease of fabrication make it suitable for accurate analysis of dielectric properties.[15,16]

Our goal is to develop a novel technique for liquid characterization in rectangular waveguides using the finite-difference-time-domain (FDTD) method enhanced with perfectly matched layer (PML) boundary conditions. The PML is essential for minimizing reflections at the boundaries, leading to more accurate simulation results. By combining experimental setups with advanced numerical models such as FDTD-PML, we aim to optimize the accuracy of liquid characterization and provide solutions for applications in telecommunications and industry. This deeper understanding of liquid dielectric properties will help minimize signal loss, improve transmission efficiency, and contribute to the development of robust communication systems.[6,17]

While this study has been performed in the X-band frequency range using a standard rectangular WR90 waveguide, it is important to emphasize the flexibility inherent in our proposed hybrid approach (2D-FDTD-PML combined with the Nelder–Mead optimization algorithm). In fact, this method can be easily generalized to higher frequency bands or adapted to different waveguide shapes. This generalization mainly involves the adaptation of boundary conditions specific to the targeted geometries and the adjustment of the spatial and temporal resolution of the numerical mesh to ensure the stability and accuracy conditions required for the simulations. The simplicity, flexibility, and adaptability of our proposed method open promising avenues for the accurate characterization of liquid materials in a wide range of industrial and scientific applications.

II. THEORY

A. Direct problem

The determination of the scattering S_{ij} parameters at the reference planes of a rectangular waveguide loaded with a multilayer dielectric material is shown in Fig. 1. The analysis considers the complex permittivity, including real and imaginary components, as well as the dielectric loss tangent, providing a comprehensive approach to evaluating the material behavior within the waveguide system.

The multilayer dielectric material consists of three layers. The first layer, with complex permittivity ε_{r1}, extends between the transverse planes at $z = L_0$ and $z = L_0 + e$. The liquid layer, with complex permittivity ε_r, is positioned between $z = L_0 + e$ and $z = L_0 + e + L$. The third layer, characterized by complex permittivity ε_{r1}, spans from $z = L_0 + e + L$ to $z = L_0 + 2e + L$.

The waveguide is assumed to operate in the dominant mode, TE_{10}. The electric field distribution within the rectangular waveguide is calculated using the 2D-FDTD method, which is based on

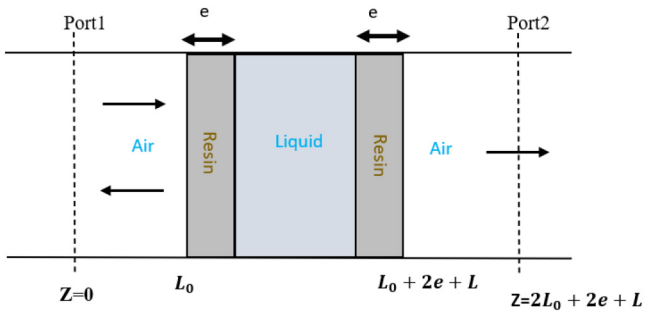

FIG. 1. Rectangular waveguide loaded with multilayer dielectric materials.

the direct discretization of the wave equations as outlined below,

$$\frac{\partial^2 E_y}{\partial t^2} = \frac{1}{\varepsilon_r \mu_r}\left(\frac{\partial^2 E_y}{\partial x^2} + \frac{\partial^2 E_y}{\partial z^2}\right). \tag{1}$$

This equation models the E_y field in a TE_{10} mode, where only the transverse electric field E_y varies.

The two-dimensional FDTD formulation for the E_y component is derived in Cartesian coordinates, following Yee's notation,[14] as outlined in Eq. (1),

$$\begin{aligned} E^{n+1}(i,k) =& 2E^n(i,k) - E^{n-1}(i,k) \\ &+ \frac{C^2\Delta t^2}{\varepsilon_r(i,k)}\left[\frac{E^n(i+1,k) + E^n(i-1,k) - 2E^n(i,k)}{\Delta x^2}\right. \\ &\left. + \frac{E^n(i,k+1) + E^n(i,k-1) - 2E^n(i,k)}{\Delta z^2}\right]. \end{aligned} \tag{2}$$

In the two-dimensional FDTD formulation, Δx and Δz represent the spatial steps along the x and z directions, while Δt is the time step. To ensure the precision of the spatial derivatives involved in calculating the electric field component, the mesh sizes in the FDTD network must be sufficiently small in comparison to the wavelength within the waveguide. Specifically, this requirement is expressed by the condition

$$\max(\Delta x, \Delta z) < \frac{\lambda_g}{m_0}, \tag{3}$$

where λ_g is the guided wavelength. Additionally, the mesh size should satisfy $10 < m_0 < 100$. This constraint ensures accurate representation of wave propagation.

To ensure the numerical stability of the 2D-FDTD algorithm, the time step Δt and the spatial increments Δx and Δz must respect the following stability stability condition:[6,16]

$$\Delta t = \frac{1}{c}\frac{1}{\sqrt{\frac{1}{\Delta x^2} + \frac{1}{\Delta z^2}}}. \tag{4}$$

Here, c refers to the speed of light in a vacuum.

In order to ensure accurate truncation of the computational mesh, perfectly matched layer (PML) boundary conditions are applied. PML is specifically designed to absorb outgoing electromagnetic waves and prevent reflections at the boundaries of the computational domain. This allows precise modeling of wave interactions with the material while avoiding artificial boundary effects. By simulating an infinite environment, PML improves the accuracy of *S*-parameter calculations, allowing reliable extraction of material properties such as permittivity and loss. This is achieved by introducing auxiliary differential equations, modifying Maxwell's equations with additional damping terms to ensure that waves are effectively absorbed at boundaries such as $z = 0$ and $z = z_{\max}$, expressed as follows:

For $z = 0$,

$$E^{n+1}(i,0) = \frac{2-\sigma_z(0)\Delta t}{2+\sigma_z(0)\Delta t}\left[2E^n(i,0) - E^{n-1}(i,0)\right] + \frac{C^2\Delta t^2}{\varepsilon_r(i,0)}\left[\frac{E^n(i+1,0)+E^n(i-1,0)-2E^n(i,0)}{\Delta x^2} + \frac{1}{\kappa_z^2(0)}\frac{E^n(i,1)-E^n(i,0)}{\Delta z^2}\right]. \quad (5)$$

For $z = z_{\max}$,

$$E^{n+1}(i,z_{\max}) = \frac{2-\sigma_z(z_{\max})\Delta t}{2+\sigma_z(z_{\max})\Delta t}\left[2E^n(i,z_{\max}) - E^{n-1}(i,z_{\max})\right] + \frac{C^2\Delta t^2}{\varepsilon_r(i,z_{\max})}\left[\frac{E^n(i+1,z_{\max})+E^n(i-1,z_{\max})-2E^n(i,z_{\max})}{\Delta x^2} + \frac{1}{\kappa_z^2(z_{\max})}\frac{E^n(i,z_{\max}-1)-E^n(i,z_{\max})}{\Delta z^2}\right]. \quad (6)$$

Here, $\sigma_z(k)$ represents the spatially varying damping parameter and $\kappa_z(k)$ is the stretching parameter in the PML region. These parameters ensure smooth absorption of outgoing waves with minimal reflection.

The effects of higher-order modes in the input waveguide can be ignored if the absorbing boundary and the input waveguide are positioned so that only the fundamental mode can propagate,

$$E(i, k_{\text{source}}) = e^{-\left(\frac{t-t_0}{\tau}\right)^2}\sin(\omega_0 t)\sin\left(\frac{\pi i\Delta x}{a}\right). \quad (7)$$

After a sufficient number of iterations, denoted as n_t, a stable field distribution is achieved, allowing the application of the DFT algorithm to obtain the desired complex field amplitude coefficient at the target frequency.

The S_{ij} parameters for the TE_{10} mode are then determined using the approach described in Ref. 17. The magnitude and phase of the mode amplitudes A and B are calculated from the following equations:

$$\int_0^a E(x,z_1)\sin\left(\frac{\pi x}{a}\right)dx = \omega_1 = A(z_1) + B(z_1), \quad (8)$$

$$\int_0^a E(x,z_1+\Delta z)\sin\left(\frac{\pi x}{a}\right)dx = \omega_2 = A(z_1)e^{-\partial j\Delta z} + B(z_1)e^{\partial j\Delta z}, \quad (9)$$

$$\int_0^a E(x,z_3)\sin\left(\frac{\pi x}{a}\right)dx = \omega_3 = A(z_3). \quad (10)$$

Here, $\sin\left(\frac{\pi x}{a}\right)$ represents the normalized modal magnetic field and $\gamma = \sqrt{\left(\frac{\omega}{c}\right)^2 - \left(\frac{\pi}{a}\right)^2}$ is the modal propagation constant. This results in the following expressions:

$$s_{11} = \frac{B}{A}(z_1) = \frac{\omega_2 - \omega_1 e^{-j\gamma\Delta z}}{\omega_1 e^{j\gamma\Delta z} - \omega_2}, \quad (11)$$

$$s_{21} = \frac{A(z_3)}{A(z_1)} = \omega_3\left(\frac{e^{j\gamma\Delta z} - e^{-j\gamma\Delta z}}{\omega_1 e^{j\gamma\Delta z} - \omega_2}\right). \quad (12)$$

Here, S_{11} represents the ratio of reflected (B) to incident (A) wave amplitudes at the input plane, while S_{21} describes the transmitted wave amplitude at the output plane relative to the input amplitude.

B. Inverse problem

This section describes the method for estimating the complex permittivity of the liquid dielectric material. This material fills the layer between two resin samples, which are placed at the ends of a rectangular waveguide to create a watertight seal. The thickness of this liquid layer is known in advance.

To achieve this, we use the Fmin function in Python,[18] which implements the Nelder–Mead sequential simplex algorithm.[19] This function is designed to solve nonlinear, unconstrained, multivariable optimization problems. It finds the minimum of a scalar function involving several variables, starting from an initial guess for the complex relative permittivity, such as $\varepsilon_r' = 1.5$ and $\varepsilon_r'' = 0.005\varepsilon_r'$, with a tolerance function of 10^{-3} and a maximum number of iterations of 100.

The objective is to minimize an error function, which is defined as the sum of the squared errors between the measured and calculated S_{ij} parameters, as described by the following equation:[5,9]

$$f(\varepsilon_r', \varepsilon_r'') = \sum \left\| S_{ijc} - S_{ijm} \right\|^2. \quad (13)$$

III. NUMERICAL RESULTS

A novel approach to improving liquid characterization in a rectangular waveguide involves the strategic use of a solid dielectric material in the transverse plane. This addition addresses the sealing challenge, ensuring that the sample remains intact and free from external interference. Additionally, placing a small hole along the longitudinal plane allows for the controlled introduction of the liquid into the waveguide as shown in Fig. 2. This setup minimizes the risk of leakage and enhances the accuracy of dielectric measurements by maintaining a stable environment for

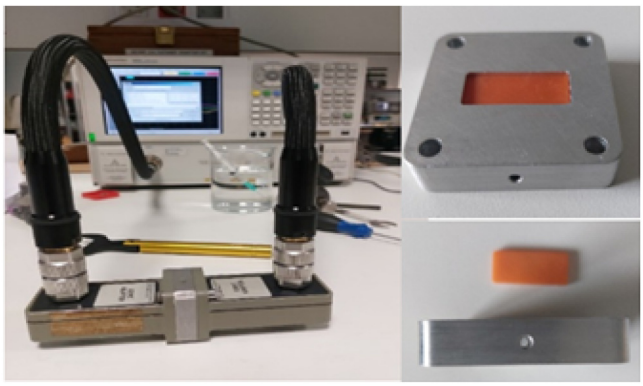

FIG. 2. Measurement system.

the liquid sample, leading to a more reliable and precise analysis of its properties.

The HFSS simulator was employed to evaluate and contrast the electromagnetic characteristics of the original WR90 waveguide with those of a modified version that features an added hole. As shown in Fig. 3, the S11 and S21 parameter results for both configurations show a strong similarity. This alignment indicates that the inclusion of the hole had minimal effect on the performance of the waveguide. Overall, the comparative analysis confirms that the structural modification had a negligible effect on the electromagnetic behavior of the waveguide.

Based on these results, we have chosen to use the WR90 waveguide with a hole in all subsequent applications. The analysis confirmed the suitability of the modified WR90 waveguide for our purposes, supporting our decision to use it consistently in subsequent research and evaluations.

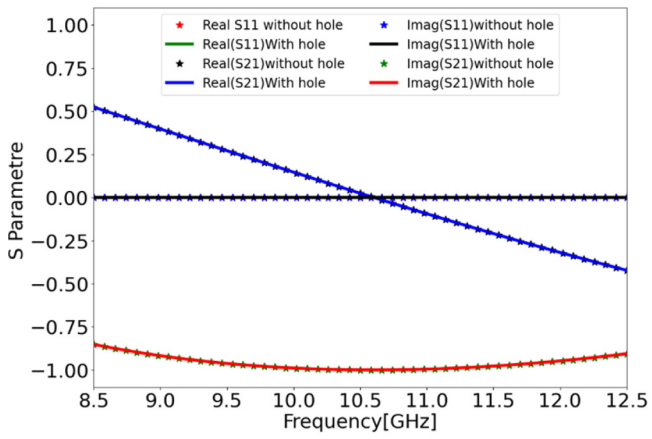

FIG. 3. A comparison of S11 and S21 parameters for standard and modified WR90 rectangular waveguide with a hole.

A. Direct problem

1. Convergence

In order to validate the accuracy and reliability of the numerical model, a convergence analysis was performed as the first step in the development of our FDTD-PML program for the empty waveguide with $L = 15\,\text{mm}$. The simulation used discretization steps of $\Delta x = 1.143\,\text{mm}$, $\Delta z = 0.1\,\text{mm}$, and a time step of $\Delta t = 0.33\,\text{ps}$ over 5000 iterations.

The convergence plot in Fig. 4 shows stable and consistent numerical behavior. This result confirms that the program is well implemented and able to accurately analyze the electromagnetic properties. The clear convergence behavior confirms the suitability of the numerical method for material characterization and S-parameter evaluation, providing a strong foundation for subsequent analysis.

2. Characterization of an empty rectangular waveguide

Following convergence validation, the direct problem was evaluated by calculating the S-parameters of a rectangular waveguide filled with air ($\varepsilon_r' = 1$, $\varepsilon_r'' = 0$) using the 2D FDTD-PML method. These calculations were compared with the results of the X-band measurement.

The simulation used discretization steps of $\Delta x = 1.143\,\text{mm}$, $\Delta z = 0.1\,\text{mm}$, and a time step of $\Delta t = 0.3323\,\text{ps}$ over 5000 iterations. This configuration ensured a stable and accurate numerical model capable of effectively characterizing the electromagnetic behavior of the waveguide with the introduced liquid. The setup demonstrated the applicability and reliability of the numerical method for X-band material characterization.

The results in Fig. 5 showed stable transmission S_{21} and minimal reflection S_{11}, confirming the efficiency of the design in the propagation of electromagnetic waves.These results are further validated by the FDTD-PML calculations, which show good agreement with the measured parameters.

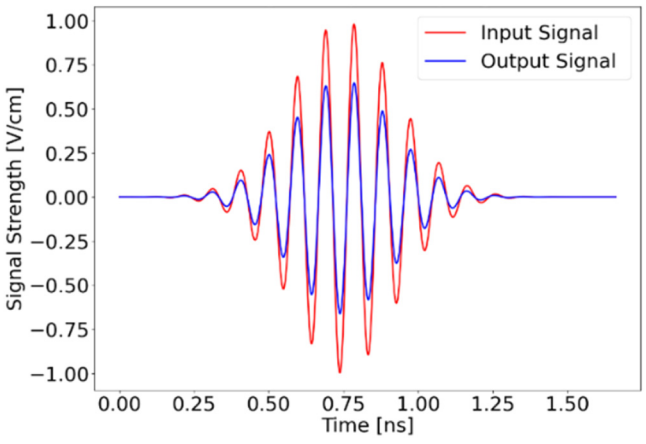

FIG. 4. Convergence plot for the numerical model validation.

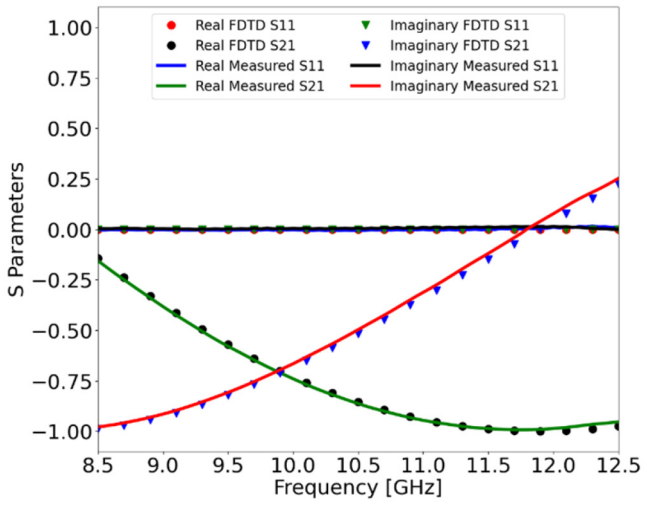

FIG. 5. S_{11} and S_{21} parameters for an empty rectangular waveguide.

3. Analysis of a rectangular waveguide closed with resin walls and an empty interior

The next step consisted of evaluating the direct problem for a rectangular waveguide modified with a strategically placed hole for liquid material introduction. Using the 2D FDTD-PML method, the S-parameters were calculated and compared with X-band measurements to verify the accuracy of the numerical model.

The waveguide was configured with 1 mm thick resin walls with complex permittivity ($\varepsilon_r' = 3.1$, $\varepsilon_r'' = 0.093$) spaced 1 mm from port 1 and 1 mm from port 2, which effectively enclosed the waveguide. This fixed prototype allowed liquid material to be introduced through the hole in the waveguide, as shown in Fig. 6.

As shown in Fig. 7, the calculated S_{11} and S_{21} parameters are in good agreement with the measured results over the frequency range, demonstrating the accuracy of the FDTD-PML method in modeling the electromagnetic behavior of the multilayer structure, including dispersion and losses. These results confirm the reliability of the FDTD-PML method for analyzing multilayer waveguide structures and its potential for simulating more complex geometries and materials.

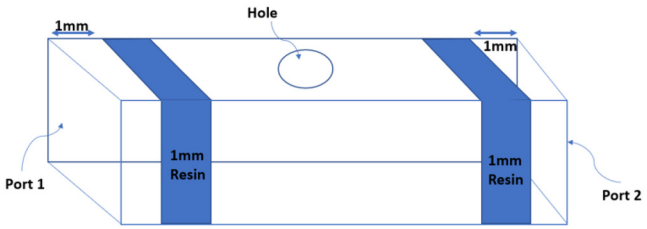

FIG. 6. Rectangular waveguide with 1 mm resin walls and an empty interior.

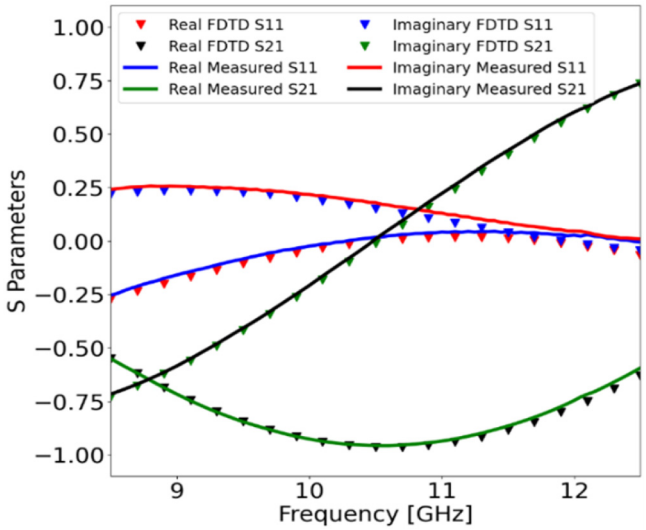

FIG. 7. S_{11} and S_{21} parameters for a rectangular waveguide closed with resin walls and an empty interior.

B. Inverse problem

1. Estimation of air complex permittivity in a RWC closed with resin walls

To estimate the complex permittivity of the air within a rectangular waveguide, which is sealed by resin walls (with complex permittivity $\varepsilon_r' = 3.1$, $\varepsilon_r'' = 0.093$), an initial guess for the air's complex permittivity ($\varepsilon_r' = 1.5$, $\varepsilon_r'' = 0.005$) was input into the numerical model. The 2D FDTD-PML method was then used to calculate S-parameters (S_{11} and S_{21}), which were compared against experimental results. Through iterative optimization, the complex

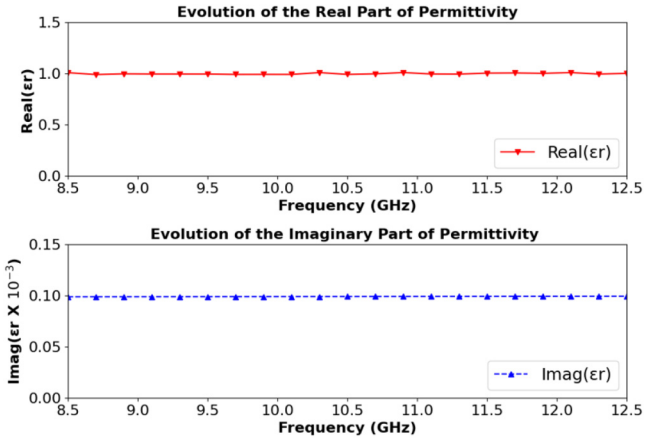

FIG. 8. Estimation of the complex permittivity of air within a rectangular waveguide closed by resin walls.

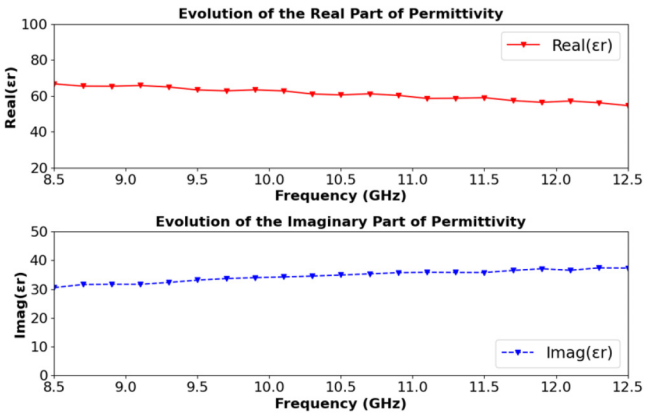

FIG. 9. Estimation of distilled water complex permittivity in a rectangular waveguide closed by resin walls.

permittivity of the air was refined until the calculated *S*-parameters closely matched the measured values.

This process confirmed the expected low dielectric constant and loss tangent of air as shown in Fig. 8, validating the ability of the model to accurately characterize low-loss materials in a resin-loaded environment.

2. Estimation of distilled water complex permittivity

For the characterization of distilled water, the rectangular waveguide was similarly configured with 1 mm thick resin walls ($\varepsilon_r' = 3.1, \varepsilon_r'' = 0.093$) and then filled with distilled water. An initial guess for the complex permittivity of the distilled water ($\varepsilon_r' = 1.5, \varepsilon_r'' = 0.005$) was provided to the numerical model. The iterative process adjusted the permittivity until the calculated parameters S_{11} and S_{21} matched the experimental measurements.

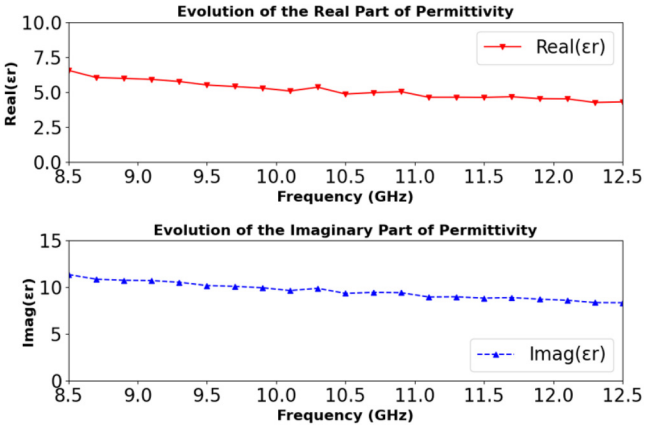

FIG. 10. Estimation of alcohol complex permittivity in a rectangular waveguide closed by resin walls.

TABLE I. Complex permittivity measured for two liquids, distilled water and alcohol, and relative errors.

	Water		Alcohol		
Liquid	ε'	ε''	ε'	ε''	Error (%)
This work	62.31	35.24	4.95	9.51	
Reference 6	58.51	33.00	–	–	6
Reference 20	61.08	34.66	5.05	9.56	2

The higher permittivity and loss tangent of water caused significant changes in the electromagnetic response that were effectively captured by the optimization process.

This analysis validated the ability of the model to handle materials with high permittivity and loss tangents, as presented in Fig. 9.

3. Estimation of alcohol permittivity in a resin-loaded waveguide

The complex permittivity of alcohol was estimated using the same waveguide configuration with resin walls enclosing the material. The initial guess for the complex permittivity of alcohol ($\varepsilon_r' = 1.5, \varepsilon_r'' = 0.005$) was entered into the model. Iterative adjustments were made to align the calculated S_{11} and S_{21} parameters with the experimental results.

The estimation of the complex permittivity shows that alcohol has a decreased electromagnetic response compared to distilled water, thus demonstrating its reduced interaction with electromagnetic fields compared to distilled water.

Figure 10 shows the ability of the model to accurately calculate the electromagnetic properties of a lossy liquid such as alcohol, illustrating its ability to handle complex material parameters.

Table I shows that the complex permittivity error is less than 6% for the liquid materials studied. The results show good agreement between the average values of the complex permittivity of the liquid materials studied and those of the same materials. These results demonstrate that this technique accurately estimates the complex permittivity of liquid dielectric materials and provides a reliable means for the characterization of liquids.[21]

IV. SUMMARY AND CONCLUSIONS

This study successfully applied a novel hybrid approach, combining the 2D-FDTD-PML method with the Nelder–Mead optimization algorithm, to estimate the complex permittivity of liquid materials in rectangular waveguides. The waveguide modification, with a strategically placed hole, effectively addressed the sealing challenges and enabled reliable liquid characterization within a multilayer structure. The calculated *S*-parameters, validated with experimental results in the X-band frequency range, confirmed the accuracy and robustness of the proposed method. The approach offers significant advantages in terms of computational efficiency, simplicity of implementation, and flexibility, as it does not depend on identical dielectric properties or precise dimensional uniformity of the sealing plugs. Additionally, it can be generalized to higher

frequency bands or different waveguide geometries by adjusting boundary conditions, mesh resolutions, and simulation parameters. This work provides a solid framework for complex permittivity estimation in multilayer systems, advances numerical modeling techniques for liquid dielectric characterization, and contributes to a deeper understanding of dielectric material behavior in controlled environments.

ACKNOWLEDGMENTS

We sincerely thank Paul García Cadelo and Eva María Cuerno García, technicians from the Departamento de Ingeniería de Comunicaciones at the Universidad de Cantabria, for their invaluable assistance in performing the measurements and providing support with all the materials and equipment used in this work.

AUTHOR DECLARATIONS

Conflict of Interest

The authors have no conflicts to disclose.

Author Contributions

Omaima Talmoudi: Data curation (equal); Formal analysis (equal); Investigation (equal); Software (equal); Validation (equal); Writing – original draft (equal); Writing – review & editing (equal). **Lahcen Ait Benali:** Data curation (equal); Methodology (equal); Software (equal); Supervision (equal); Validation (equal). **Jaouad Terhzaz:** Methodology (equal); Supervision (equal); Validation (equal); Writing – review & editing (equal). **Abdelwahed Tribak:** Methodology (equal); Supervision (equal); Validation (equal). **Tomás Fernández-Ibáñez:** Supervision (equal); Validation (equal).

DATA AVAILABILITY

The data that support the findings of this study are available from the corresponding author upon reasonable request.

REFERENCES

[1]J. Krupka, "Microwave measurements of electromagnetic properties of materials," Materials **14**(17), 5097 (2021).
[2]Y. Tao, B. Yan, D. Fan, N. Zhang, S. Ma, L. Wang *et al.*, "Structural changes of starch subjected to microwave heating: A review from the perspective of dielectric properties," Trends Food Sci. Technol. **99**, 593–607 (2020).
[3]J. K. Pakkathillam, B. T. Sivaprakasam, J. Poojali, C. V. Krishnamurthy, and K. Arunachalam, "Tailoring antenna focal plane characteristics for a compact free-space microwave complex dielectric permittivity measurement setup," IEEE Trans. Instrum. Meas. **70**, 1–12 (2020).
[4]L. A. Benali, J. Terhzaz, A. Tribak, and A. M. Sanchez, "2D-FDTD method to estimate the complex permittivity of multilayer dielectric materials at Ku-band frequencies," Prog. Electromagn. Res. M **91**, 155–164 (2020).
[5]O. Talmoudi, L. A. Benali, J. Terhzaz, A. Tribak, and T. F. Ibanez, Determination of distilled water dielectric constant by 2D-FDTD method at X-band frequencies," in *IRASET* (IEEE, 2024).
[6]U. C. Hasar and A. Cansiz, "Simultaneous complex permittivity and thickness evaluation of liquid materials from scattering parameter measurements," Microwave Opt. Technol. Lett. **52**(1), 75–78 (2010).
[7]H. Ebara, T. Inoue, and O. Hashimoto, "Measurement method of complex permittivity and permeability for a powdered material using a waveguide in microwave band," Sci. Technol. Adv. Mater. **7**(1), 77 (2006).
[8]A. Saad-Falcon, Z. Zhang, D. Ryoo, J. Dee, R. S. Westafer, and J. C. Gumbart, "Extraction of dielectric permittivity from atomistic molecular dynamics simulations and microwave measurements," J. Phys. Chem. B **126**(40), 8021–8029 (2022).
[9]L. A. Benali, A. Tribak, J. Terhzaz, and T. F. Ibanez, "New FDTD method to estimate the dielectric constant and loss tangent of a bilayer dielectric material at x-band frequencies," Int. J. Microwave Opt. Technol., **18**(6), 575–582 (2023).
[10]J. Terhzaz, H. Ammor, A. Assir, and A. Mamouni, "Application of the FDTD method to determine complex permittivity of dielectric materials at microwave frequencies using a rectangular waveguide," Microwave Opt. Technol. Lett. **49**(8), 1964–1968 (2007).
[11]T. Mosavirik, V. Nayyeri, M. Hashemi, M. Soleimani, and O. M. Ramahi, "Direct permittivity reconstruction from power measurements using a machine learning aided method," IEEE Trans. Microwave Theory Tech. **71**(10), 4437–4448 (2023).
[12]J. Qin, Z. Liu, M. Ma, and Y. Li, "Machine learning approaches for permittivity prediction and rational design of microwave dielectric ceramics," J. Materiomics **7**(6), 1284–1293 (2021).
[13]J. Ma, J. Tang, K. Wang, L. Guo, Y. Gong, and S. Wang, "Complex permittivity characterization of liquid samples based on a split ring resonator (SRR)," Sensors **21**(10), 3385 (2021).
[14]D. V. Krupezevic, V. J. Brankovic, and F. Arndt, "The wave-equation FD-TD method for the efficient eigenvalue analysis and S-matrix computation of waveguide structures," IEEE Trans. Microwave Theory Tech. **41**(12), 2109–2115 (1993).
[15]L. A. Benali, J. Terhzaz, A. Tribak, and A. Mediavilla, "Complex permittivity estimation for each layer in a bi-layer dielectric material at Ku-band frequencies," Prog. Electromagn. Res. M **70**, 109–116 (2018).
[16]U. C. Hasar, "Permittivity measurement of thin dielectric materials from reflection-only measurements using one-port vector network analyzers," Prog. Electromagn. Res. **95**, 365–380 (2009).
[17]J. Elmajid, J. Terhzaz, H. Ammor, M. Chaïbi, and M. Sánchez, "A new method to determine the complex permittivity and complex permeability of dielectric materials at X-band frequencies," Int. J. Microwave Opt. Technol. **10**, 1 (2015).
[18]P. O. U. Guide, Python, Version 3.10.4 (2022).
[19]J. A. Nelder and R. Mead, "A simplex method for function minimization," Comput. J. **7**, 308–313 (1965).
[20]A. Chathurika, M. Halgamuge, P. Farrell, and S. Skafidas, "An *ab-initio* computational method to determine dielectric properties of biological materials," Sci. Rep. **3**, 1796 (2013).
[21]C. Yang, K. Ma, and J.-G. Ma, "A noniterative and efficient technique to extract complex permittivity of low-loss dielectric materials at terahertz frequencies," IEEE Anten. Wireless Propag. Lett. **18**(10), 1971–1975 (2019).